MATERIALS PHYSICS AND MECHANICS RESEARCH ARTICLE

Submitted: November 16, 2025 **Revised: January 20, 2026** **Accepted: March 12, 2026**

Identification of the variable characteristics of a functionally graded elastic pipe with voids

S.A. Nesterov ✉

Vladikavkaz Scientific Center of the Russian Academy of Sciences, North Ossetia-Alania, Russia

✉ 1079@list.ru

ABSTRACT

Using the Cowin-Nunziato model, a coefficient inverse problem for inhomogeneous poroelastic bodies is formulated, and operator equations of the 1st kind for its solution are derived. As an example, an inverse problem for a functionally graded elastic pipe with voids is considered using additional information measured in the domain of transient loading. To solve the direct transient problem, a combined method is used: transition to the Laplace transform space, followed by solution of the boundary value problem using the shooting method and inversion using an expansion in shifted Legendre polynomials. The solution to the direct problem was verified by comparing it with the solution obtained in the finite element package FlexPDE for a homogeneous pipe. The influence of the heterogeneity laws of the Lamé moduli, coupling modulus, pore diffusion modulus, density, and pore stiffness modulus on the radial displacement was investigated. For reconstruction of physical and mechanical characteristics the iteration approach is applied. Two methods discretization of operator equations (a collocation method and a projection method) are proposed. The initial approximation is defined among the constants as the average of the maximum and minimum values of the material properties. Refinement of physical and mechanical characteristics in projection method was carried out in stages: (1) among constants; (2) linear functions; (3) quadratic functions. Computational experiments were conducted to reconstruct variable properties both at internal points of the pipe and in the class of power functions. A comparative analysis of the effectiveness of the proposed discretization schemes is performed.

KEYWORDS

elastic pipe with voids • Cowin-Nunziato theory • functionally graded material • identification variable physical and mechanical properties • integral equation 1st kind • iterative approach

Citation: Nesterov SA. Identification of the variable characteristics of a functionally graded elastic pipe with voids. *Materials Physics and Mechanics*. 2026;54(2): 41–56.
http://dx.doi.org/10.18149/MPM.5422026_4

Introduction

Functionally graded porous materials (FGPM) represent a new class of composites in which the volume fraction of pores and mechanical properties vary smoothly in space [1–3]. Due to this, an optimal combination of lightness, strength, and the ability to withstand extreme thermal and mechanical loads is achieved. The development of additive technologies, in particular 3D printing, has opened new prospects for manufacturing products from FGPM with complex internal structures [2,4]. Cylindrical bodies made of FGPM are widely used in various engineering fields: oil and gas, chemical, aerospace industries, power engineering, and biomedicine.

However, the widespread adoption of such materials is hindered by the lack of reliable non-destructive testing methods to verify the compliance of the actual property distribution with the design one. The problem is exacerbated by the fact that

Publisher: Peter the Great St. Petersburg Polytechnic University

the production of FGPM faces a number of technological difficulties, such as instability of the interfacial bond due to differences in the physical and chemical properties of the components. Therefore, an important task is to control the inhomogeneity laws, for example, using non-destructive technologies and solving coefficient inverse problems (CIP) for elastic bodies with pores.

Based on the micro-dilatational Cowin-Nunziato model [5], problems of deformation of cylindrical bodies, including homogeneous [6–8], composite [9,10], and inhomogeneous bodies [11–13], have been investigated. The Cowin-Nunziato theory contains a number of non-classical parameters, whose values are not available in reference books, which limits the practical use of this theory. In [14–17], theoretical approaches for determining non-classical parameters using various concepts are proposed. In [14,15], the concept of "penalized micro-dilatation" was developed, establishing a connection between the microstructural characteristics of a porous material and the macroscopic parameters of the model. By homogenizing a representative volume with explicit pore modeling, analytical expressions for non-classical moduli in terms of pore size and porosity were obtained. The main limitation of this approach is the idealization of the microstructure (assumption of spherical isolated pores), which limits its applicability for real materials with complex pore morphology. In [16], combinations of parameters that can be uniquely determined from various types of experiments were identified, and corresponding experimental schemes were proposed. However, the work is limited to static problems for homogeneous materials and does not account for the influence of measurement errors. In [17], a methodology was developed for determining porosity parameters based on solving the contact problem of indenting a rigid indenter into a porous half-space. The obtained analytical solution allows determining non-classical moduli from measured contact characteristics. The advantage of the method is its locality and the possibility of using standard equipment, but it determines properties only of the near-surface layer and is not applicable for dynamic problems.

The approaches [14–17] for finding the non-classical parameters of the Cowin-Nunziato theory are limited to homogeneous materials and do not account for functional grading, which is critically important for modern composites obtained by additive technologies. This work fills this gap. In comparison with previous works of the Vatulyan scientific school [18–23], where inverse problems of thermoelasticity and Biot poroelasticity are studied, the proposed approach for the first time allows identifying non-classical parameters of materials with microstructure based on two methods for solving operator equations: the collocation method and the projection method. Unlike works [24–29], which use resource-intensive gradient methods or heuristic optimization algorithms, the proposed approach reduces the inverse problem to solving linear integral equations at each iteration. Furthermore, the problem of local minima is absent due to the use of Newton-Kantorovich linearization.

The aim of the work is the development of an iterative method for solving the coefficient inverse problem for a functionally graded porous pipe within the framework of the Cowin-Nunziato model, allowing the determination of the variation laws of physical and mechanical characteristics from additional information on transient displacement fields on the outer surface.

The main results obtained include: (1) operator equations for the Cowin-Nunziato model relating corrections to the sought functions to the displacement field; (2) an iterative scheme for reconstructing the properties of a poroelastic pipe using two discretization methods (collocation and projection); (3) identification of different sensitivity of displacements to different material characteristics, which explains the accuracy of their reconstruction; (4) consideration of thermodynamic constraints ensuring the positive definiteness of the elastic potential. The developed method for solving the coefficient inverse problem can be used for non-destructive testing of cylindrical products made of FGPM obtained by 3D printing methods.

Problem of vibrations of inhomogeneous poroelastic bodies

Let us consider the transient vibrations of an inhomogeneous elastic body with voids. To describe the mechanical behavior of such an object, we will use the Cowin-Nunziato theory [5]. It is important to emphasize that the Cowin-Nunziato theory is an averaged continuum theory in which the real discrete structure of the porous material is replaced by a continuous medium with an additional degree of freedom – micro-dilation ψ, interpreted as the change in the volume fraction of the material matrix at the considered point of the medium. On the other hand, the micro-dilation function is defined as $\psi = -\Delta n$, where $\Delta n = n - n_0$ is the increment of porosity from its value in the undeformed state n_0. The applicability range of the linear Cowin-Nunziato model is limited by the following conditions: (1) pores are small, numerous, and uniformly distributed; (2) initial porosity is small; (3) deformations and porosity increments are small.

For a linear anisotropic elastic material with voids, the constitutive relations have the form [5]: $\sigma_{ij} = c_{ijkl}\varepsilon_{kl} + D_{ijk}\psi_{,k} + \beta_{ij}\psi$ are the components of the classical stress tensor, $h_i = a_{ij}\psi_{,j} + D_{ijk}\varepsilon_{jk}$ are the components of the non-classical stress vector, and $g = -\left(\xi\psi + \omega\frac{\partial\psi}{\partial t} + \beta_{ij}\varepsilon_{ij}\right)$ is the internal volume force. Here, $\varepsilon_{ij} = 0.5(u_{i,j} + u_{j,i})$ are the components of the strain tensor, u_i are the components of the displacement vector, c_{ijkl} are the components of the elastic moduli tensor, β_{ij} and D_{ijk} are the components of the second- and third-order coupling tensor, respectively, a_{ij} are the components of the pore diffusion tensor, ρ is the density, ξ is the pore stiffness modulus, ω is the micro-viscoelastic modulus.

The non-classical parameters used in the Cowin-Nunziato model have a clear physical meaning. The interpretation of these parameters depends significantly on the symmetry class of the material. In the general anisotropic case, which is described by the tensors in constitutive relations, the coupling between the skeleton deformation and the porosity change is characterized by a second-rank tensor β_{ij}. This means that the change in pore volume may depend on the direction of the applied macroscopic strain: for example, stretching in one direction might increase porosity, while stretching in another direction could decrease it. Similarly, the pore diffusion modulus, which governs the gradient energy associated with porosity changes, becomes a second-rank tensor a_{ij} in anisotropic media. This implies that the "influence zone" of a local porosity disturbance is directionally dependent, with pores interacting more strongly along certain crystallographic or structural directions than others. The pore stiffness ξ, however,

remains a scalar even in anisotropic materials, as it represents the isotropic resistance to a purely volumetric change in porosity at the microscale, independent of direction. The micro-viscoelastic modulus ω also retains its scalar nature, characterizing the intrinsic dissipation associated with the rate of porosity change. The change in pore volume is not a perfectly elastic process. Part of the energy is dissipated as heat due to internal friction during pore wall movement.

In the specific case of an isotropic material, which is the focus of the present study of a functionally graded pipe, these tensors simplify dramatically. The coupling tensor reduces to a scalar β multiplied by the Kronecker delta δ_{ij}, indicating that volumetric strain and porosity change are directly and proportionally coupled, with no directional preference. The pore diffusion tensor similarly simplifies to a scalar a times the identity, meaning that porosity disturbances diffuse equally in all directions. Thus, for the isotropic pipe, the physical meaning of the moduli becomes particularly clear: the coupling modulus β describes the mutual influence of skeleton strains and porosity changes; the pore diffusion modulus a characterizes the range of elastic interaction between pores; and the micro-viscoelastic modulus ω characterizes dissipative losses associated with changes in porosity over time.

Let a poroelastic body have a volume V and a piecewise smooth boundary $S_u \cup S_\sigma = S$, $S_\psi \cup S_h = S$, where S_u, S_ψ, S_σ, S_h are the parts of the body's surface on which the boundary conditions for the displacement, the porosity function, and classical and nonclassical stresses, respectively, are specified. The formulation of the dynamic poroelasticity problem within the Cowin-Nunziato model, in the absence of external body forces, is as follows [5]:

$$\sigma_{ij,j} - \rho \frac{\partial^2 u_i}{\partial t^2} = 0,\ h_{i,i} + g - \chi \frac{\partial^2 \psi}{\partial t^2} = 0,$$
$$\sigma_{ij} n_j|_{S_\sigma} = w_i(t),\ h_i n_i|_{S_h} = 0, \quad (1)$$
$$u_i|_{S_u} = u_i^0,\ \psi|_{S_\psi} = \psi_0,\ u_i(x,0) = \frac{\partial u_i}{\partial t}(x,0) = \psi(x,0) = \frac{\partial \psi}{\partial t}(x,0) = 0.$$

Here χ is the equilibrated inertia modulus, $w_i(t)$ are components of the load vector. The equilibrated inertia modulus χ characterizes the inertial properties of the microstructure is a measure of how quickly porosity can change in dynamic processes. Under impact loading, pores cannot instantly change their volume, so the equilibrated inertia parameter determines the time delay of this process. The direct problem consists of computing the functions u_i and ψ from Eq. (1) given known characteristics a_{ij}, β_{ij}, D_{ijk}, c_{ijkl}, ρ, ξ, ω, χ.

Operator equations for solving the inverse problem

We assume the moduli ω, χ are constant. The inverse problem consists of finding the functions q (a_{ij}, β_{ij}, D_{ijk}, c_{ijkl}, ρ, ξ) from Eq. (1) using additional information, measured on S_σ:

$$u_i|_{S_\sigma} = f_i(x,t),\ t \in [c_1, c_2],\ i = 1..3. \quad (2)$$

The inverse Eqs. (1) are (2) is a nonlinear problem, since the sought coefficients appear in the differential operators. To solve it, an iterative approach, analogous to the Newton-Kantorovich method, is applied. Linearization is carried out using the perturbation method within the framework of the weak formulation of the problem. To solve the CIP (1)–(2) we obtain an operator equation that establishes a relationship between the functions q and the boundary fields $u_i|_{S_\sigma}$.

First, we obtain the weak formulation of problem (1). Substituting the expanded expressions for the σ_{ij}, h_i, g, into problem (1), and applying the Laplace transform, setting $\tilde{u}_i^0 = 0, \tilde{\psi}_0 = 0$, we obtain:

$$\begin{gathered}\left(c_{ijkl}\tilde{u}_{k,l} + \beta_{ij}\tilde{\psi} + D_{ijk}\tilde{\psi}_{,k}\right)_{,j} - p^2\bar{\rho}\tilde{u}_i = 0,\\ \left(a_{ij}\tilde{\psi}_{,i} + D_{ijk}\tilde{u}_{i,k}\right)_{j} - (\xi + p\omega + p^2\chi)\tilde{\psi} - \beta_{ij}\tilde{u}_{i,j} = 0,\\ \tilde{\sigma}_{ij}n_j|_{S_\sigma} = \widetilde{w}_i, \quad \tilde{h}_j n_j|_{S_h} = 0, \tilde{u}_i|_{S_u} = 0, \tilde{\psi}|_{S_\psi} = 0.\end{gathered} \tag{3}$$

We multiply first equations (3) by $\tilde{v}_i$, second equations (3) by $\kappa_1\tilde{\vartheta}$. Here, $\tilde{v}_i$ and $\tilde{\vartheta}$ are test functions, satisfying the principal boundary conditions $\tilde{v}_i|_{S_u} = 0, \quad \tilde{\vartheta}|_{S_\psi} = 0$. We integrate the resulting products over V. Next, we multiply the boundary condition on the part S_σ by $\kappa_2\tilde{v}_i$ and integrate over S_σ. Summing all the obtained integrals into a single expression and equating it to zero, we get:

$$\begin{gathered}\int_V \left(c_{ijkl}\tilde{u}_{k,l} + \beta_{ij}\tilde{\psi} + D_{ijk}\tilde{\psi}_{,k}\right)_{,j}\tilde{v}_i dV + \kappa_1\int_V\left(a_{ij}\tilde{\psi}_{,i} + D_{ijk}\tilde{u}_{i,k}\right)_{j}\tilde{\vartheta}dV\ p^2\int_V \rho\tilde{u}_i\,\tilde{v}_i dV -\\ -\kappa_1\int_V(\xi + p\omega + p^2\chi)\tilde{\psi}\,\tilde{\vartheta}dV - \kappa_1\int_V \beta_{ij}\tilde{u}_{i,j}\,\tilde{\vartheta}dV +\\ +\kappa_2\int_{S_\sigma}(\tilde{\sigma}_{ij}n_j - \widetilde{w}_i)\tilde{v}_i dS = 0.\end{gathered} \tag{4}$$

Next, applying the Gauss-Ostrogradsky theorem to the first two integrals in Eq. (4), we obtain:

$$\begin{gathered}-\int_V c_{ijkl}\,\tilde{u}_{i,j}\tilde{v}_{k,l}dV - p^2\int_V \rho\tilde{u}_i\,\tilde{v}_i dV - \int_V \beta_{ij}\left(\tilde{\psi}\tilde{v}_{i,j} + \kappa_1\tilde{\vartheta}\tilde{u}_{i,j}\right)dV -\\ \int_V D_{ijk}\left(\tilde{\psi}_{,k}\tilde{v}_{i,j} + \kappa_1\tilde{\vartheta}_{,k}\tilde{u}_{i,j}\right)dV - \kappa_1\int_V \xi\tilde{\psi}\tilde{\theta}\,dV -\\ -\kappa_1(\omega + \chi p)p\int_V \tilde{\psi}\tilde{\theta}\,dV - \kappa_1\int_V \beta_{ij}\tilde{u}_{i,j}\,\tilde{\vartheta}dV + \int_{S_\sigma}\left((1+\kappa_2)\tilde{\sigma}_{ij}n_j - \kappa_2\widetilde{w}_i\right)\tilde{v}_i dS = 0.\end{gathered} \tag{5}$$

Setting in Eq. (5) $\kappa_1 = 1, \kappa_2 = -1$, we obtain the weak formulation of problem (1):

$$-\int_V \xi\tilde{\psi}\tilde{\theta}\,dV - -\int_V D_{ijk}\left(\tilde{\psi}_{,k}\tilde{v}_{i,j} + \tilde{\vartheta}_{,k}\tilde{u}_{i,j}\right)dV - (\omega + \chi p)p\int_V \tilde{\psi}\tilde{\theta}\,dV + \int_{S_\sigma}\widetilde{w}_i\,\tilde{v}_i dS = 0. \tag{6}$$

Two states of the poroelastic body are considered within the same weak formulation Eq. (6). The first state is the true state with exact, but unknown characteristics: coefficients $c_{ijkl}^{true}, \xi^{true}, \rho^{true}, \xi^{true}, a_{ij}^{true}, \beta_{ij}^{true}, D_{ijk}^{true}, \omega^{true}, \chi^{true}$ and fields $\tilde{u}_i^{true}, \tilde{\psi}^{true}, \tilde{v}_i^{true}$:

$$\begin{gathered}-\int_V c_{ijkl}^{true}\,\tilde{u}_{i,j}^{true}\tilde{v}_{k,l}^{true}dV - p^2\int_V \rho^{true}\tilde{u}_i^{true}\,\tilde{v}_i^{true}dV -\\ \int_V \beta_{ij}^{true}\left(\tilde{\psi}^{true}\tilde{v}_{i,j}^{true} + \tilde{\vartheta}^{true}\tilde{u}_{i,j}^{true}\right)dV - \int_V a_{ij}^{true}\,\tilde{\psi}_{,i}^{true}\tilde{\theta}_{,j}^{true}dV -\\ -\int_V \xi^{true}\tilde{\psi}^{true}\tilde{\theta}^{true}\,dV - \int_V D_{ijk}^{true}\left(\tilde{\psi}_{,k}^{true}\tilde{v}_{i,j}^{true} + \tilde{\vartheta}_{,k}^{true}\tilde{u}_{i,j}^{true}\right)dV -\\ -(\omega^{true} + \chi^{true}p)p\int_V \tilde{\psi}^{true}\tilde{\theta}^{true}\,dV +\\ +\int_{S_\sigma}\widetilde{w}_i\,\tilde{v}_i^{true}dS = 0.\end{gathered} \tag{7}$$

The second state is the approximate state at the $(n-1)$-th iteration, which is characterized by the coefficients known at this step $c_{ijkl}^{(n-1)}, \xi^{(n-1)}, \rho^{(n-1)}, a_{ij}^{(n-1)}, \beta_{ij}^{(n-1)}, D_{ijk}^{(n-1)}, \omega^{(n-1)}, \chi^{(n-1)}$ and the corresponding fields $\tilde{u}_i^{(n-1)}, \tilde{\psi}^{(n-1)}\ \tilde{v}_i^{(n-1)}$:

$$\begin{gathered}-\int_V c_{ijkl}^{(n-1)}\,\tilde{u}_{i,j}^{(n-1)}\tilde{v}_{k,l}^{(n-1)}dV - p^2\int_V \rho^{(n-1)}\tilde{u}_i^{(n-1)}\,\tilde{v}_i^{(n-1)}dV -\\ -\int_V \beta_{ij}^{(n-1)}\left(\tilde{\psi}^{(n-1)}\tilde{v}_{i,j}^{(n-1)} + +\tilde{\vartheta}^{(n-1)}\tilde{u}_{i,j}^{(n-1)}\right)dV -\\ -\int_V a_{ij}^{(n-1)}\,\tilde{\psi}_{,i}^{(n-1)}\tilde{\theta}_{,j}^{(n-1)}dV - \int_V \xi^{(n-1)}\tilde{\psi}^{(n-1)}\tilde{\theta}^{(n-1)}\,dV -\\ -\int_V D_{ijk}^{(n-1)}\left(\tilde{\psi}_{,k}^{(n-1)}\tilde{v}_{i,j}^{(n-1)} + \tilde{\vartheta}_{,k}^{(n-1)}\tilde{u}_{i,j}^{(n-1)}\right)dV -\\ -\left(\omega^{(n-1)} + \chi^{(n-1)}p\right)p\int_V \tilde{\psi}^{(n-1)}\tilde{\theta}^{(n-1)}\,dV + \int_{S_\sigma}\widetilde{w}_i\,\tilde{v}_i^{(n-1)}dS = 0.\end{gathered} \tag{8}$$

Suppose that the true values of the coefficients and fields can be represented as the sum of approximate values and small corrections that need to be found at the n-th step. Let

us write this for the elastic moduli and displacements: $c_{ijkl}^{true} \approx c_{ijkl}^{(n)} = c_{ijkl}^{(n-1)} + \delta c_{ijkl}^{(n-1)}$, $\tilde{u}_i^{true} \approx \tilde{u}_i^{(n)} = \tilde{u}_i^{(n-1)} + \delta\tilde{u}_i^{(n-1)}$. The remaining moduli and fields are expanded similarly. Here, the superscript $(n-1)$ corresponds to quantities obtained at the previous iteration, and the index n – to quantities obtained at the current iteration.

Subtract relation Eq. (8) from Eq. (7), assuming $\tilde{v}_i^{true} = \tilde{u}_i^{(n-1)}$, $\tilde{v}_i^{(n-1)} = \tilde{u}_i^{(n)}$. The resulting difference contains products of coefficients and fields, for example, $c_{ijkl}^{(n-1)}\tilde{u}_{i,j}^{(n-1)}\tilde{u}_{k,l}^{(n-1)} + c_{ijkl}^{(n-1)}\delta\tilde{u}_{i,j}^{(n-1)}\tilde{u}_{k,l}^{(n-1)} + \delta c_{ijkl}^{(n-1)}\tilde{u}_{i,j}^{(n-1)}\tilde{u}_{k,l}^{(n-1)} + \delta c_{ijkl}^{(n-1)}\delta\tilde{u}_{i,j}^{(n-1)}\tilde{u}_{k,l}^{(n-1)} - -c_{ijkl}^{(n-1)}\tilde{u}_{i,j}^{(n-1)}\tilde{u}_{k,l}^{(n-1)} - c_{ijkl}^{(n-1)}\tilde{u}_{i,j}^{(n-1)}\delta\tilde{u}_{k,l}^{(n-1)}$. Linearization consists of discarding nonlinear second-order small terms in the form of products of corrections $\delta c_{ijkl}^{(n-1)}\delta\tilde{u}_{i,j}^{(n-1)}\tilde{u}_{k,l}^{(n-1)}$. After canceling terms and linearization, only the expression $\delta c_{ijkl}^{(n-1)}\tilde{u}_{i,j}^{(n-1)}\tilde{u}_{k,l}^{(n-1)}$ remains. Performing similar actions for the remaining products, we obtain a linear Fredholm integral equation of the 1st kind, relating the unknown coefficient corrections to the residual of the boundary data:

$$\int_V \delta c_{ijkl}^{(n-1)}\,\tilde{u}_{i,j}^{(n-1)}\tilde{u}_{k,l}^{(n-1)}dV + p^2\int_V \delta\rho^{(n-1)}\left(\tilde{u}_i^{(n-1)}\right)^2 dV + \int_V \delta\beta_{ij}^{(n-1)}\tilde{\psi}^{(n-1)}\tilde{u}_{i,j}^{(n-1)}\,dV +$$
$$+\int_V \delta a_{ij}^{(n-1)}\,\tilde{\psi}_{,i}^{(n-1)}\tilde{\psi}_{,j}^{(n-1)}dV + \int_V \delta D_{ijk}^{(n-1)}\tilde{\psi}_{,i}^{(n-1)}\tilde{u}_{j,k}^{(n-1)}\,dV + \int_V \delta\xi^{(n-1)}\left(\tilde{\psi}^{(n-1)}\right)^2 dV = \quad (9)$$
$$= -\int_{S_\sigma}\tilde{w}_i\left(\tilde{f}_i - \tilde{u}_i^{(n-1)}\right)dS,\ p \in 0,\infty).$$

If only one of the physical and mechanical characteristics is unknown, then by setting in Eq. (9) the corrections of all characteristics except the sought one to zero, we obtain the following Fredholm integral equations of the 1st kind:

$$\begin{aligned}
&\int_V \delta c_{ijkl}^{(n-1)}\,\tilde{u}_{i,j}^{(n-1)}\tilde{u}_{k,l}^{(n-1)}dV = -\int_{S_\sigma}\tilde{w}_i\left(\tilde{f}_i - \tilde{u}_i^{(n-1)}\right)dS, p \in 0,\infty),\\
&p^2\int_V \delta\rho^{(n-1)}\left(\tilde{u}_i^{(n-1)}\right)^2 dV = -\int_{S_\sigma}\tilde{w}_i\left(\tilde{f}_i - \tilde{u}_i^{(n-1)}\right)dS, p \in 0,\infty),\\
&\int_V \delta\beta_{ij}^{(n-1)}\tilde{u}_{i,j}^{(n-1)}\,\tilde{\psi}^{(n-1)}dV = -\int_{S_\sigma}\tilde{w}_i\left(\tilde{f}_i - \tilde{u}_i^{(n-1)}\right)dS, p \in 0,\infty),\\
&\int_V \delta D_{ijk}^{(n-1)}\tilde{u}_{i,j}^{(n-1)}\,\tilde{\psi}_{,k}^{(n-1)}dV = -\int_{S_\sigma}\tilde{w}_i\left(\tilde{f}_i - \tilde{u}_i^{(n-1)}\right)dS, p \in 0,\infty),\\
&\int_V \delta a_{ij}^{(n-1)}\,\tilde{\psi}_{,i}^{(n-1)}\tilde{\psi}_{,j}^{(n-1)}dV = -\int_{S_\sigma}\tilde{w}_i\left(\tilde{f}_i - \tilde{u}_i^{(n-1)}\right)dS, p \in 0,\infty),\\
&\int_V \delta\xi^{(n-1)}\left(\tilde{\psi}^{(n-1)}\right)^2 dV = -\int_{S_\sigma}\tilde{w}_i\left(\tilde{f}_i - \tilde{u}_i^{(n-1)}\right)dS, p \in 0,\infty).
\end{aligned} \quad (10)$$

Formulation and solution of the direct problem for a pipe

As an example, we investigate a problem for an inhomogeneous isotropic elastic pipe with voids. The inner surface of the tube $r = r_1$ is free from loads, and non-stationary vibrations are caused by applying a transient loading $\sigma_{rr}(r_2,t) = -w(t)$ to its outer surface $r = r_2$. Setting in Eq. (1) $c_{ijkl} = \lambda\delta_{ij}\delta_{lk} + \mu\left(\delta_{ik}\delta_{jl} + \delta_{il}\delta_{jk}\right)$, $a_{ij} = a\delta_{ij}$, $\beta_{ij} = \beta\delta_{ij}$, $D_{ijk} = 0$ and converting to a cylindrical coordinate system, we obtain:

$$\begin{aligned}
&\frac{\partial\sigma_{rr}}{\partial r} + \frac{\sigma_{rr}-\sigma_{\varphi\varphi}}{r} - \rho\frac{\partial^2 u_r}{\partial t^2} = 0,\ r_1 \le r \le r_2,\ t \ge 0,\\
&\frac{\partial h_r}{\partial r} + \frac{h_r}{r} - \left(\xi - \omega\frac{\partial}{\partial t} + \chi\frac{\partial^2}{\partial t^2}\right)\psi - \beta\left(\frac{u_r}{r} + \frac{\partial u_r}{\partial r}\right) = 0,\ r_1 \le r \le r_2,\ t \ge 0,\\
&\sigma_{rr}(r_1,t) = h_r(r_1,t) = 0,\ \sigma_{rr}(r_2,t) = -w(t),\ \ h_r(r_2,t) = 0,\\
&u_r(r,0) = \frac{\partial u_r}{\partial t}(r,0) = \psi(r,0) = \frac{\partial\psi}{\partial t}(r,0) = 0,
\end{aligned} \quad (11)$$

where $\sigma_{rr} = (\lambda+2\mu)\frac{\partial u_r}{\partial r} + \lambda\frac{u_r}{r} + \beta\psi$, $\sigma_{\varphi\varphi} = (\lambda+2\mu)\frac{u_r}{r} + \lambda\frac{\partial u_r}{\partial r} + \beta\psi$, $h_r = a\frac{\partial\psi}{\partial r}$.

For generality, we introduce the following dimensionless parameters and functions: $\eta = \frac{r}{r_2}$ $\eta_0 = \frac{r_1}{r_2}$, $\tau = \frac{t}{t_0}$, $t_0 = \sqrt{\frac{\rho_0}{\mu_0}} r_2$, $U = \frac{u_r}{r_2}$, $\Phi = \frac{\xi_0}{\beta_0}\psi$, $H_r = \frac{h_r}{\beta_0 r_2}$, $\Omega_{ij} = \frac{\sigma_{ij}}{\mu_0}$, $W = \frac{w}{\mu_0}$, $\bar{\lambda} = \frac{\lambda}{\mu_0}$, $\bar{\mu} = \frac{\mu}{\mu_0}$, $\bar{\rho} = \frac{\rho}{\rho_0}$, $\bar{\xi} = \frac{\xi}{\xi_0}$, $\bar{\beta} = \frac{\beta}{\beta_0}$, $\bar{a} = \frac{a}{\xi_0 r_2^2}$, $\varepsilon_1 = \frac{\omega}{\xi_0 t_0}$, $\varepsilon_2 = \frac{\chi}{\xi_0 t_0^2}$, $\delta_0 = \frac{\beta_0^2}{\mu_0 \xi_0}$. Here, μ_0, ξ_0, β_0, ρ_0 are characteristic values of the corresponding physical and mechanical characteristics.

For the physical realizability of the Cowin-Nunziato model, the following conditions for positive definiteness of the elastic potential must be satisfied [5]: $\mu(r) > 0, 3\lambda(r) + 2\mu(r) > 0$, $\xi(r) > 0$, $a(r) > 0$, $\xi(r)\big(3\lambda(r) + 2\mu(r)\big) - 3\beta^2(r) > 0$ or in dimensionless form $\bar{\mu}(\eta) > 0, 3\bar{\lambda}(\eta) + 2\bar{\mu}(\eta) > 0, \bar{\xi}(\eta) > 0, \bar{a}(\eta) > 0, \bar{\xi}(\eta)\left(3\bar{\lambda}(\eta) + 2\bar{\mu}(\eta)\right) - 3\delta_0\bar{\beta}^2(\eta) > 0.$

The dimensionless formulation of problem (11) becomes:

$$\begin{aligned}
&\frac{\partial \Omega_{rr}}{\partial \eta} + \frac{\Omega_{rr} - \Omega_{\varphi\varphi}}{\eta} - \bar{\rho}\frac{\partial^2 U}{\partial \tau^2} = 0, \quad \eta_0 \le \eta \le 1, \tau \ge 0,\\
&\frac{\partial H_r}{\partial \eta} + \frac{H_r}{\eta} - \left(\bar{\xi} - \varepsilon_1\frac{\partial}{\partial \tau} + \varepsilon_2\frac{\partial^2}{\partial \tau^2}\right)\Phi - \bar{\beta}\left(\frac{U}{\eta} + \frac{\partial U}{\partial \eta}\right) = 0, \quad \eta_0 \le \eta \le 1, \tau \ge 0,\\
&\Omega_{rr}(\eta_0, \tau) = 0, \; H_r(\eta_0, \tau) = 0, \Omega_{rr}(1, \tau) = -W(\tau), \; H_r(1, \tau) = 0,\\
&U(\eta, 0) = \frac{\partial U}{\partial \tau}(\eta, 0) = \Phi(\eta, 0) = \frac{\partial \Phi}{\partial \tau}(\eta, 0) = 0.
\end{aligned} \tag{12}$$

Since problem (12) is non-stationary, to transition to ordinary differential equations, we apply the Laplace transform with respect to time to Eq. (12):

$$\begin{aligned}
&\frac{d\tilde{\Omega}_{rr}}{d\eta} + 2\bar{\mu}\left(\frac{d\tilde{U}}{d\eta} - \frac{\tilde{U}}{\eta}\right) - p^2\bar{\rho}\tilde{U} = 0, \; \eta_0 \le \eta \le 1, p \ge 0,\\
&\frac{d\tilde{H}_r}{d\eta} + \frac{\tilde{H}_r}{\eta} - \left(\bar{\xi} - \varepsilon_1 p + \varepsilon_2 p^2\right)\tilde{\Phi} - \bar{\beta}\left(\frac{\tilde{U}}{\eta} + \frac{d\tilde{U}}{d\eta}\right) = 0, \eta_0 \le \eta \le 1, p \ge 0,\\
&\tilde{\Omega}_{rr}(\eta_0, p) = 0, \; \tilde{H}_r(\eta_0, p) = 0, \; \tilde{\Omega}_{rr}(1, p) = -\tilde{W}(p), \; \tilde{H}_r(1, p) = 0.
\end{aligned} \tag{13}$$

Next, system (13), considering that, $\tilde{\Omega}_{rr} = \left(\bar{\lambda} + 2\bar{\mu}\right)\frac{d\tilde{U}}{d\eta} + \bar{\lambda}\frac{\tilde{U}}{\eta} + \delta_0\bar{\beta}\tilde{\Phi}$, $\tilde{H}_r = \bar{a}\frac{d\tilde{\Phi}}{d\eta}$, after some transformations, is reduced to a canonical system of ordinary differential equations of 1st order with variable coefficients:

$$\begin{aligned}
&\frac{d\tilde{\Phi}}{d\eta} = \frac{\tilde{H}_r}{\bar{a}},\\
&\frac{d\tilde{H}_r}{d\eta} = -\frac{\tilde{H}_r}{\eta} + \left(\bar{\xi} + p\varepsilon_1 + p^2\varepsilon_2\right)\tilde{\Phi} + \frac{\tilde{\Omega}_{rr}}{\bar{\lambda}+2\bar{\mu}} + \frac{2\bar{\mu}\tilde{U}}{(\bar{\lambda}+2\bar{\mu})\eta},\\
&\frac{d\tilde{\Omega}_{rr}}{d\eta} = -\frac{2\bar{\mu}\tilde{\Omega}_{rr}}{(\bar{\lambda}+2\bar{\mu})\eta} + \left(p^2\bar{\rho} + \frac{2\bar{\mu}}{\eta^2}\left(1 + \frac{\bar{\lambda}}{\bar{\lambda}+2\bar{\mu}}\right)\right)\tilde{U} + \frac{2\bar{\mu}\delta_0\bar{\beta}\tilde{\Phi}}{(\bar{\lambda}+2\bar{\mu})\eta},\\
&\frac{d\tilde{U}}{d\eta} = \frac{1}{\bar{\lambda}+2\bar{\mu}}\left(\tilde{\Omega}_{rr} - \frac{\bar{\lambda}}{\eta}\tilde{U} - \delta_0\bar{\beta}\tilde{\Phi}\right).
\end{aligned} \tag{14}$$

System (14) is supplemented by boundary conditions:

$$\tilde{\Omega}_{rr}(\eta_0, p) = 0, \tilde{H}_r(\eta_0, p) = 0, \tilde{\Omega}_{rr}(1, p) = -\tilde{W}(p), \tilde{H}_r(1, p) = 0. \tag{15}$$

We solve the boundary value problem in the transform domain (14) and (15) using the shooting method. For this, we consider two auxiliary Cauchy problems, consisting of the canonical system (14) and two sets of conditions: (1) $\tilde{\Phi}^I(\eta_0, p) = 1$, $\tilde{U}^I(\eta_0, p) = 0$, $\tilde{\Omega}^I_{rr}(\eta_0, p) = 0$, $\tilde{H}^I_r(\eta_0, p) = 0$; (2) $\tilde{\Phi}^{II}(\eta_0, p) = 0$, $\tilde{U}^{II}(\eta_0, p) = 1$, $\tilde{\Omega}^{II}_{rr}(\eta_0, p) = 0$, $\tilde{H}^{II}_r(\eta_0, p) = 0$.

We solve the auxiliary Cauchy problems using the Runge-Kutta method for an integer set of values of the Laplace transform parameter p. We compose the expressions: $\tilde{\Phi} = \alpha_1\tilde{\Phi}^I + \alpha_2\tilde{\Phi}^{II}$, $\tilde{U} = \alpha_1\tilde{U}^I + \alpha_2\tilde{U}^{II}$, $\tilde{\Omega}_{rr} = \alpha_1\tilde{\Omega}^I_{rr} + \alpha_2\tilde{\Omega}^{II}_{rr}$, $\tilde{H}_r = \alpha_1\tilde{H}^I_r + \alpha_2\tilde{H}^{II}_r$.

The constants α_1 and α_2 are determined from the conditions $\tilde{\Omega}_{rr}(1,p) = -\tilde{W}(p)$, $\tilde{H}_r(1,p) = 0$.

To invert the transforms $\tilde{F}$ ($\tilde{\Phi}$, $\tilde{U}$, $\tilde{\Omega}_{rr}$, $\tilde{H}_r$), we use the method of expanding the original function into a series in shifted Legendre polynomials [30]:

$$F(\tau) = \sum_{s=0}^{\infty}(2s+1)\, a_s P_s^*(e^{-\tau}). \quad (16)$$

Here, P_s^* are the shifted Legendre polynomials.

Verification of the solution obtained by the proposed method was carried out by comparison with a finite element method (FEM) in the FlexPDE 7 package for the case of a homogeneous pipe. The computational domain in the FlexPDE package in Cartesian coordinates was the cross-section of the pipe – a ring with an inner radius of 0.7 and an outer radius of 1.0. Quadratic triangular elements with six nodes and an automatic adaptive mesh refinement mechanism were used. The mesh was constructed using the parameter *ngrid = 30*, which sets the initial number of cells in each dimension. The calculation error criterion was set by the parameter *errlim = 1e-4*. The final computation time was 1 dimensionless second. The proposed method (shooting method + inversion of the Laplace transform using shifted Legendre polynomials) was implemented in the computer algebra system Maple 15. It used 30 nodes along the radius and 50 terms of the Legendre series.

Table 1 presents the values of the radial displacement of the pipe, computed on the outer surface $\eta = 1$ using the shooting method and FEM for some time points under the load $W(\tau) = H(\tau)$ ($H(\tau)$ is Heaviside function) with dimensionless parameters $\bar{a} = 0.4$, $\varepsilon_1 = \varepsilon_2 = 0.001$, $\delta_0 = 0.1$, $\bar{\rho} = 1$, $\bar{\mu} = 1$, $\bar{\lambda} = 0.8$, $\bar{\xi} = 1$, $\eta_0 = 0.7$. The relative error γ_1 was determined using the relation $\gamma_1 = \frac{|U_{FEM}(1,\tau_j) - U_{SH}(1,\tau_j)|}{U_{FEM}(1,\tau_j)} \cdot 100\%$, where $U_{FEM}(1,\tau_j)$ is the displacement computed in FlexPDE, $U_{SH}(1,\tau_j)$ is the displacement found by the proposed method at a given time points τ_j.

Table 1. Values of the radial displacement, computed on the outer surface of the pipe under the load $W(\tau) = H(\tau)$

Time points τ	FlexPDE	Proposed method			
		$s_1 = 40$	Relative error, %	$s_1 = 65$	Relative error, %
0.01	0.0058	0.0061	5.17	0.0059	1.72
0.05	0.0302	0.0312	3.31	0.0306	1.32
0.1	0.0613	0.0624	1.79	0.0619	0.98
0.5	0.4719	0.4793	1.57	0.4759	0.85
1	1.3793	1.3942	1.08	1.3866	0.53

From Table 1, it follows that the deviation error from the FEM for times $\tau \geq 0.01$ does not exceed 2 % with $s = 65$ terms of the series in expansion (16). The computation time for the direct problem using the proposed method in Maple 15 is 24 seconds, and in the FlexPDE package it is 8 sec. It should be noted that the choice of the Maple system for calculations is not driven by the pursuit of record speed for solving a single direct problem, but by the need to solve a complex inverse problem in an environment where we can fully control and adapt to the mathematical apparatus. In the inverse problem, we do not simply solve the same equation; we constantly change the material properties (the sought functions). Implementing such feedback in FlexPDE is extremely difficult, while in Maple it is a natural process.

The influence of physical and mechanical characteristics on the radial displacement was investigated. Figure 1 shows the influence of polynomial inhomogeneity laws on displacement under the load $W(\tau) = H(\tau)$ with dimensionless parameters $\eta_0 = 0.7$, $\delta_0 = 0.1$, $\varepsilon_1 = \varepsilon_2 = 0.001$, $\bar{a} = 0.2$, $\bar{\lambda} = 0.8$. Here, solid lines represent graphs for a homogeneous pipe, dots – for an inhomogeneous pipe with $\bar{\mu}(\eta) = 1 + \eta^2$ (Fig. 1(a)), $\bar{\rho}(\eta) = 1 + \eta^2$ (Fig. 1(b)).

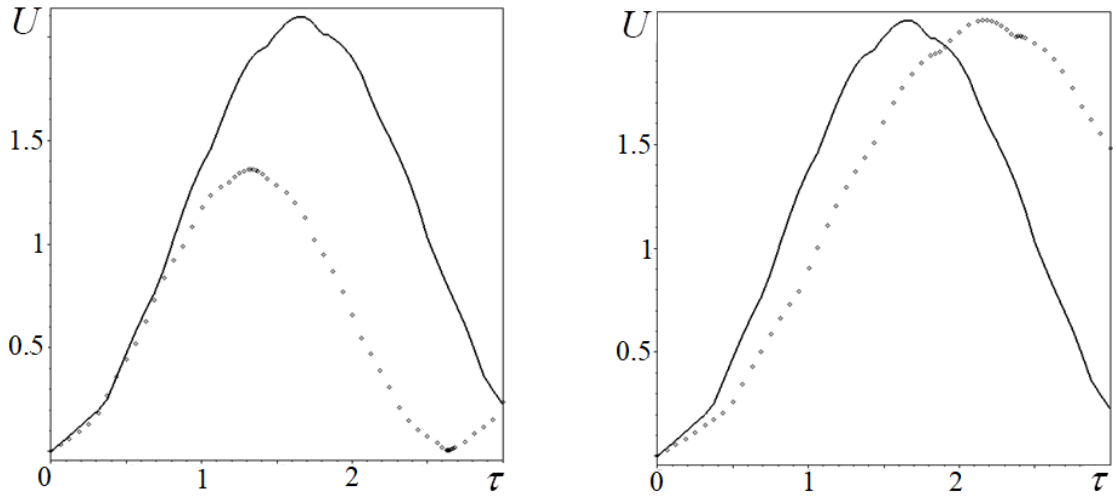

Fig. 1. Influence of different heterogeneity laws of the shear modulus (a) and density (b) on the radial displacement of the pipe's outer surface

Figure 1 shows that that the shear modulus and density significantly influence the change in displacement. During the computations, it was also found that the influence of the moduli $\bar{\lambda}$, $\bar{\beta}$ and $\bar{\xi}$ is substantially lower, and the coefficient $\bar{a}$ has practically no influence. Thus, information about the radial displacement of the outer surface at different times can serve as additional information for identifying the moduli $\bar{\lambda}$, $\bar{\mu}$, $\bar{\rho}$, $\bar{\beta}$, $\bar{\xi}$.

Iterative scheme for solving the inverse problem for the pipe

The inverse problem is to determine one of the characteristics $\bar{q}$ $(\bar{\lambda}, \bar{\mu}, \bar{\rho}, \bar{\beta}, \bar{\xi})$ from Eq. (12) on the basis of some additional information at the boundary $\eta = 1$:

$$U(1,\tau) = f(\tau),\ \tau \in [\bar{c}_1, \bar{c}_2]. \tag{17}$$

To solve the CIP (12), (17) for an isotropic pipe, we first obtain operator equations in the transform domain. For this, we convert equations (10) to a cylindrical coordinate system, setting $a_{ij} = 0$, $\beta_{ij} = \beta\delta_{ij}$, $D_{ijk} = 0$, $c_{ijkl} = \lambda\delta_{ij}\delta_{lk} + \mu\left(\delta_{ik}\delta_{jl} + \delta_{il}\delta_{jk}\right)$.

The nondimensionalized operator equations in the transform domain for a porous pipe take the form:

$$\begin{gathered}
\int_{\eta_0}^{1} \delta\bar{\lambda}^{(n-1)} \left(\frac{d\widetilde{U}^{(n-1)}}{d\eta} + \frac{\widetilde{U}^{(n-1)}}{\eta}\right)^2 \eta d\eta = -\widetilde{W}\left(\tilde{f}(p) - \widetilde{U}^{(n-1)}(1,p)\right),\ p \in 0,\infty),\\
\int_{\eta_0}^{1} \delta\bar{\mu}^{(n-1)} \left(\left(\frac{\partial\widetilde{U}^{(n-1)}}{\partial\eta}\right)^2 + \left(\frac{\widetilde{U}^{(n-1)}}{\eta}\right)^2\right)\eta d\eta = -\widetilde{W}\left(\tilde{f}(p) - \widetilde{U}^{(n-1)}(1,p)\right),\ p \in 0,\infty),\\
p^2 \int_{\eta_0}^{1} \delta\bar{\rho}^{(n-1)}\left(\widetilde{U}^{(n-1)}\right)^2 \eta d\eta = -\widetilde{W}\left(\tilde{f}(p) - \widetilde{U}^{(n-1)}(1,p)\right),\ p \in 0,\infty),\\
\int_{\eta_0}^{1} \delta\bar{\xi}^{(n-1)}\left(\widetilde{\Phi}^{(n-1)}\right)^2 \eta d\eta = -\widetilde{W}\left(\tilde{f}(p) - \widetilde{U}^{(n-1)}(1,p)\right),\ p \in 0,\infty),\\
\int_{\eta_0}^{1} \delta\bar{\beta}^{(n-1)} \frac{d\widetilde{U}^{(n-1)}}{d\eta}\widetilde{\Phi}^{(n-1)}\,\eta d\eta = -\widetilde{W}\left(\tilde{f}(p) - \widetilde{U}^{(n-1)}(1,p)\right),\ p \in 0,\infty).
\end{gathered} \tag{18}$$

To solve the inverse problem in the actual space let us apply to the Eqs. (18) the convolution theorem and the theorem on the differentiation of the original. Under the load $W(\tau) = H(\tau)$, the operator equations in the actual space can be represented as:

$$\int_{\eta_0}^{1} \delta\bar{q}^{(n-1)} M_s(\eta,\tau)\eta d\,\eta = -\left(f(\tau) - U^{(n-1)}(1,\tau)\right),\ s = 1..5,\ \tau \in [\bar{c}_1, \bar{c}_2]. \quad (19)$$

Here, $M_s(z,\tau)$ are kernels obtained by inverting the kernels of the integral equations in the transform domain (18). The form of the kernels $M_1(\eta,\tau)$, $M_2(\eta,\tau)$ and $M_3(\eta,\tau)$, for finding the corrections $\delta\bar{\lambda}^{(n-1)}$, $\delta\bar{\mu}^{(n-1)}$, $\delta\bar{\rho}^{(n-1)}$ respectively, coincides with [20,23]. The kernels for finding the corrections of pore stiffness modulus and the coupling modulus have the form: $M_4(\eta,\tau) = \delta_0 \int_0^{\tau} \Phi^{(n-1)}(\eta,\tau_1) \frac{\partial \Phi^{(n-1)}(\eta,\tau-\tau_1)}{\partial \tau_1} d\tau_1$, $M_5(\eta,\tau) = \delta_0 \int_0^{\tau} \frac{\partial U^{(n-1)}}{\partial \eta}(\eta,\tau_1)^{(n-1)} \frac{\partial \Phi^{(n-1)}(\eta,\tau-\tau_1)}{\partial \tau_1} d\tau_1$.

The kernels of the integral equations (19) represent the specific energy accumulated in the material by a given time due to the action of the corresponding mechanism (shear energy, energy of volumetric expansion of the skeleton, energy of pore volume change, energy of porosity gradient and kinetic energy). In all equations, the right-hand side is the same. This means that to separate the contributions of different moduli, we rely solely on the different dynamics of the change in the kernels $M_s(\eta,\tau)$ over time. This emphasizes the importance of sensitivity analysis and the selection of informative time intervals.

In this work, finite-dimensional approximation of the integral equations (19)was carried out by two methods. The first method is the collocation method. For that, we introduce a uniform partition of the segment $[\eta_0, 1]$ into $m_1 + 1$ segments by the points $\eta_i = \Delta d(i-1), i = 1..m_1 + 1,$ where $\Delta d = \frac{(1-\eta_0)}{m_1}$ is the subinterval. Then, we introduce a uniform partition of the time interval $[\bar{c}_1, \bar{c}_2]$ into m_2 segments by the points $\tau_j = \Delta t(j-1), j = 1..m_2$, where $\Delta t = (\bar{c}_2 - \bar{c}_1)/m_2$ is the subinterval.

The second method is the projection method. In this case, the physical and mechanical characteristics were represented as expansions in power functions:

$$\delta\bar{q}^{(n-1)}(\eta) = \sum_{i=1}^{N} b_i^{(n-1)} r_i(\eta), r_i(\eta) = \eta^{i-1}, i = 1..N. \quad (20)$$

Substituting expansions (20) into Eq. (19), we obtain a system of linear algebraic equations (SLAE):

$$\sum_{i=1}^{N} b_i^{(n-1)} A_{ij}^{(n-1)} = D_j^{(n-1)}, j = 1..M. \quad (21)$$

Here, $A_{ij}^{(n-1)} = \int_{\eta_0}^{1} r_i(\eta) M_s^{(n-1)}(\eta,\tau_j)\eta d\eta$, $D_j^{(n-1)} = -\left(f(\tau_j) - U^{(n-1)}(1,\tau_j)\right)$, $s = 1..5$, $i = 1..N, j = 1..M$.

To solve the ill-conditioned SLAE (21), the Tikhonov regularization method [31] is used. This method allows finding an approximate solution to the system of equations by minimizing the Tikhonov smoothing functional, which takes into account the deviation of the solution from a given function and the regularization parameter. The optimal value of the regularization parameter α_{reg} is selected at each iteration, based on the balance condition between the residual of the solution and its norm, taking into account the known noise level in the input data.

The iterative reconstruction process starts with the initial approximation $\bar{q}^{(0)} = (\bar{q}_- + \bar{q}_+)/2$. Here $\bar{q}_-$ and $\bar{q}_+$ are the minimum and maximum values of the sought function, respectively. To ensure the fulfillment of thermodynamic constraints at each

iteration, the step damping method is proposed. After calculating the correction $\delta\bar{q}^{(n-1)}$ from the solution of the integral equations (19) at the $(n-1)$-th iteration, the damping coefficient $\kappa \in 0{,}1$ is determined such that the updated values of the physical and mechanical characteristics $\bar{q}^{(n)}(\eta) = \bar{q}^{(n-1)}(\eta) + \kappa\delta\bar{q}^{(n-1)}(\eta)$ satisfy all positive definiteness conditions at all nodes. The choice of κ is carried out as follows. We set $\kappa = 1$ and check the fulfillment of all constraints for the trial solution $\bar{q}^{(n)}(\eta) = \bar{q}^{(n-1)}(\eta) + \kappa\delta\bar{q}^{(n-1)}(\eta)$. If the constraints are satisfied, we accept $\kappa = 1$. Otherwise, a binary search procedure is implemented on the interval $0{,}1$: the interval is sequentially halved, and for each trial $\kappa = (0.5{,}0.25{,}0.125, \dots)$ the fulfillment of the constraints is checked.

The exit from the iterative process was carried out when reaching the maximum number of iterations $n = 30$ or the residual functional:

$$J^{(n-1)} = \int_{\bar{c}_1}^{\bar{c}_2} \left(f(\tau) - U^{(n-1)}(1,\tau)\right)^2 d\tau, \tag{22}$$

which reached the threshold value $\theta = 10^{-4}$. In this case, when using the second method of discretizing the integral equations (19), the physical and mechanical characteristics are refined stepwise.

Stage 1 (constant approximation). The sought characteristics are assumed to be constant along the radius: $\bar{q}(\eta) = q_0$. The inverse problem is solved for the scalar quantities q_0. The obtained values q_0^* are fixed as the initial approximation for the next stage.

Stage 2 (linear approximation). The characteristics are sought in the form $\bar{q}(\eta) = q_0 + q_1\eta$. The initial approximation vector is formed as $[q_0^*, 0]$, i.e., the linear coefficient is taken as zero. Next, an iterative process is performed, at each step of which corrections to both coefficients q_0 and q_1 are determined. After convergence, the obtained values q_0^{**}, q_1^{**} are used in the next stage.

Stage 3 (quadratic approximation). The characteristics are represented in the form $\bar{q}(\eta) = q_0 + q_1\eta + q_2\eta^2$. Initial approximation: $[q_0^{**}, q_1^{**}, 0]$. All three coefficients are refined jointly. Result: final values q_0, q_1, q_2.

The transition between stages was carried out upon fulfillment of the residual functional stabilization criterion: $\frac{|J^{(n)} - J^{(n-1)}|}{J^{(n-1)}} < \varepsilon_J$, $\varepsilon_J = 10^{-3}$ (the relative change in the residual functional in the last iterations of the current stage does not exceed 10^{-3}).

Identification results

This section presents the results of reconstructing the physical and mechanical characteristics of a poroelastic pipe. In calculations, it is accepted: $W(\tau) = H(\tau)$, $\eta_0 = 0.6$. One of the dimensionless characteristics was reconstructed, the others were assumed equal to 1, except for $\delta_0 = 0.4$, $\bar{a} = 0.5$.

Input data was modeled by solving the direct problem (12) using the shooting method under exact laws of change in the material properties. The maximum reconstruction error was determined using the relation $\gamma_2 = \frac{|\bar{q}_{ex}(\eta) - \bar{q}_{rec}(\eta)|}{\max\limits_{\eta\in[\eta_0,1]} \bar{q}_{ex}(\eta)} \cdot 100\ \%$, where $\bar{q}_{ex}(\eta)$ is the exact law, $\bar{q}_{rec}(\eta)$ is the reconstructed one.

The shear modulus and density, which have a dominant influence on the dynamics at the initial moments, were identified from early times on the interval $[\bar{c}_1, \bar{c}_2] = [0.1{,}0.8]$, the remaining moduli – at later times, for example, the Lamé modulus $\bar{\lambda}$ – on the interval

$[\bar{c}_1, \bar{c}_2] = [0.6,1.4]$, modulus $\bar{\xi}$ – on the interval $[\bar{c}_1, \bar{c}_2] = [0.8,2]$. In this case, from 7 to 12 measurement points were selected within the informative intervals. It should be noted that all dimensionless characteristics used in the computational experiments satisfy the conditions of thermodynamic correctness at any point in the interval $\eta \in [\eta_0, 1]$. The convergence of the iterative process for different characteristics and approximation methods was investigated. The results of the study are presented in Table 2.

Table 2. Convergence of the iterative process for various reconstructed characteristics

Reconstructed characteristic	Method	Number of Iterations	Final values of the residual functional
$\bar{\mu} = 0.46e^{5.5(\eta-\eta_0)}$	Collocation	14	$8.3 \cdot 10^{-5}$
$\bar{\mu} = 0.46e^{5.5(\eta-\eta_0)}$	Projection	10	$5.3 \cdot 10^{-5}$
$\bar{\mu} = 2.4 - 7.3\eta + 6.6\eta^2$	Collocation	13	$8.9 \cdot 10^{-5}$
$\bar{\mu} = 2.4 - 7.3\eta + 6.6\eta^2$	Projection	10	$6.4 \cdot 10^{-5}$
$\bar{\rho} = 1.3 + 2.6\eta - 2.2\eta^2$	Collocation	12	$7.5 \cdot 10^{-5}$
$\bar{\rho} = 1.3 + 2.6\eta - 2.2\eta^2$	Projection	9	$4.9 \cdot 10^{-5}$
$\bar{\lambda} = 0.6 + 2.2e^{-6.3(\eta-\eta_0)}$	Collocation	28	$9.8 \cdot 10^{-5}$
$\bar{\lambda} = 0.6 + 2.2e^{-6.3(\eta-\eta_0)}$	Projection	19	$6.1 \cdot 10^{-5}$
$\bar{\lambda} = 1 + 4\eta - 3.3\eta^2$	Projection	24	$9.4 \cdot 10^{-5}$
$\bar{\xi} = 2.7 - 3\eta + 2.4\eta^2$	Projection	30	$2.6 \cdot 10^{-3}$

From Table 2, it follows that the iterative identification process requires from 9 to 30 iterations depending on the type of characteristic being reconstructed. Thus, the characteristics $\bar{\mu}$ and $\bar{\rho}$ are reconstructed quite quickly in 9–14 iterations due to their strong influence on displacements. For the Lamé parameter $\bar{\lambda}$, more iterations are required (19–28) and the reconstruction error is higher due to weak sensitivity. When reconstructing the non-classical modulus $\bar{\xi}$, the exit from the iterative process occurred due to the maximum number of iterations – 30, while the value of the residual functional turned out to be significantly higher than the threshold value. The computation time per iteration ranged from 50 sec to 1.5 min, and the total reconstruction time for one characteristic ranged from 7 to 45 min.

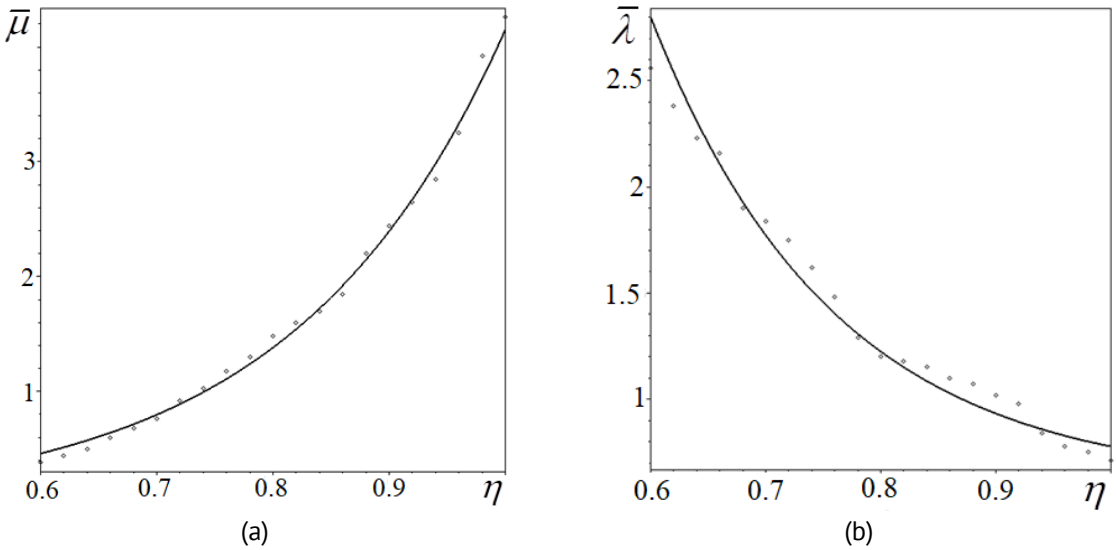

(a) (b)

Fig. 2. Results of pointwise reconstruction of functions: (a) $\bar{\mu} = 0.46e^{5.5(\eta-\eta_0)}$; (b) $\bar{\lambda} = 0.6 + 2.2e^{-6.3(\eta-\eta_0)}$. The solid line and dots represent the exact and restored functions, respectively

Figure 2 shows the results of pointwise reconstruction of characteristics: (a) $\bar{\mu} = 0.46e^{5.5(\eta-\eta_0)}$; (b) $\bar{\lambda} = 0.6 + 2.2e^{-6.3(\eta-\eta_0)}$. Figure 3 presents the results of reconstructing functions: (a) $\bar{\mu} = 2.4 - 7.3\eta + 6.6\eta^2$; (b) $\bar{\rho} = 1.3 + 2.6\eta - 2.2\eta^2$ within the class of quadratic functions (20). Figure 4 shows the results of reconstructing the pore stiffness modulus: (a) $\bar{\xi} = 2.7 - 3\eta + 2.4\eta^2$; (b) $\bar{\lambda} = 1 + 4\eta - 3.3\eta^2$ within the class of quadratic functions (20).

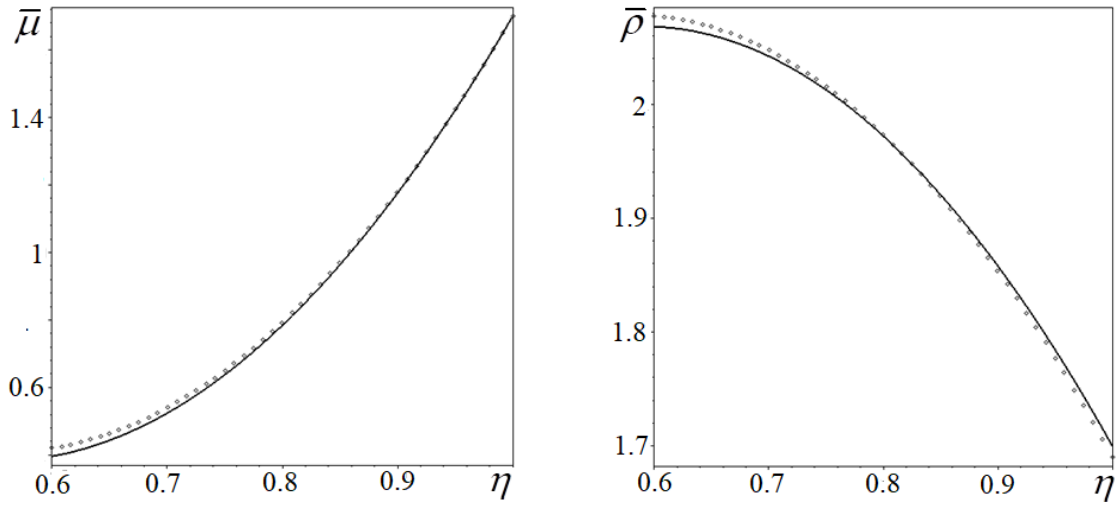

(a) (b)

Fig. 3. Results of reconstructing characteristics in the class of quadratic functions: (a) $\bar{\mu} = 2.4 - 7.3\eta + 6.6\eta^2$; (b) $\bar{\rho} = 1.3 + 2.6\eta - 2.2\eta^2$. The solid line and dots represent the exact and restored functions, respectively

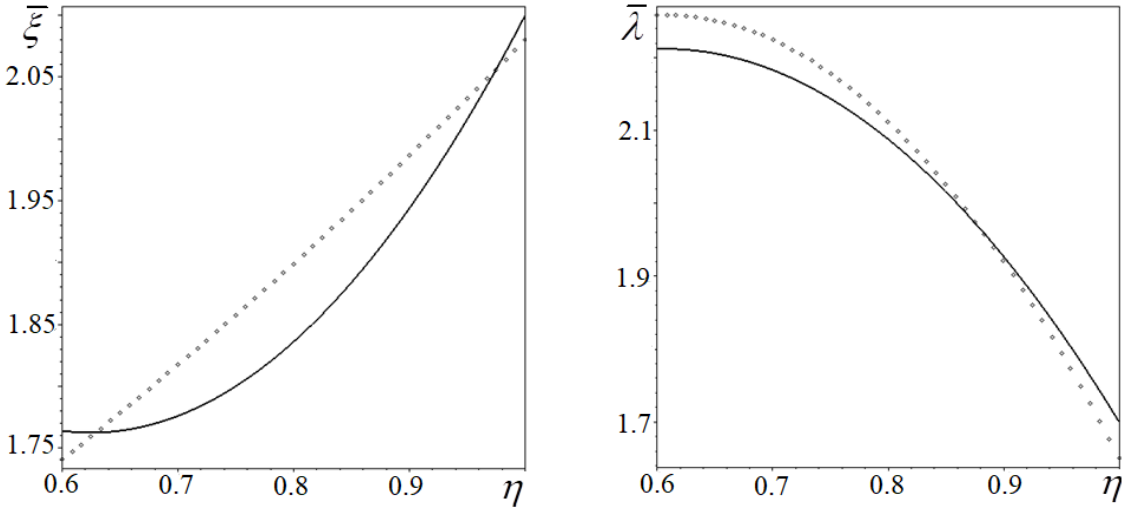

(a) (b)

Fig. 4. Results of reconstructing characteristics in the class of quadratic functions: (a) $\bar{\xi} = 2.7 - 3\eta + 2.4\eta^2$; (b) $\bar{\lambda} = 1 + 4\eta - 3.3\eta^2$. The solid line and dots represent the exact and restored functions, respectively

From Figs. 2–4, it follows that the moduli $\bar{\lambda}$, $\bar{\xi}$ are reconstructed significantly worse than $\bar{\mu}$, $\bar{\rho}$, which is related to their lesser influence on the radial displacement. The stability of the reconstruction to noise in the input data was investigated. The input information (radial displacement on the outer surface) was noised according to the

formula: $f_\omega(\tau) = f(\tau)(1 + \vartheta\zeta)$, where ϑ is the noise level, ζ is a random variable with a uniform distribution law on the interval $[-1,1]$.

Table 3 presents the results of reconstructing the function $\bar{\mu} = 0.46e^{5.5(\eta-\eta_0)}$ when approximating the operator equations by the collocation method, both in the absence of noise ($\vartheta = 0$) and in the presence of a 1 % measurement error ($\vartheta = 0.01$).

Table 3. Results of reconstructing the function $\bar{\mu} = 0.46e^{5.5(\eta-\eta_0)}$ depending on the presence and absence of noise in the input information

Coordinate η	Exact value $\bar{\mu}$	Reconstructed value $\bar{\mu}$		Relative reconstruction error, %	
		$\vartheta = 0$	$\vartheta = 0.01$	$\vartheta = 0$	$\vartheta = 0.01$
0.6	0.46	0.42	0.4	8.7	13
0.64	0.57	0.53	0.50	7	12.3
0.68	0.71	0.68	0.76	4.2	7
0.72	0.89	0.91	0.95	2.3	6.7
0.76	1.11	1.16	1.21	4.5	9
0.8	1.38	1.44	1.52	4.4	10.2
0.84	1.72	1.70	1.83	1.2	6.4
0.88	2.15	2.18	2.01	1.4	6.5
0.92	2.67	2.73	2.58	2.2	3.4
0.96	3.33	3.27	3.17	1.8	4.8
1.0	4.15	4.27	4.32	2.9	4

From Table 3, it follows that the maximum reconstruction error with 1 % input data noise increased from 8.7 to 13 %, which is an acceptable result for engineering applications. Similarly, computational experiments were conducted for other physical and mechanical characteristics of the pipe when approximating the operator equations by the collocation method. It was found that with a measurement error of 1 %, the reconstruction error for characteristics $\bar{\mu}$ and $\bar{\rho}$ does not exceed 11 %, and for the Lamé modulus $\bar{\lambda}$ – 35 %, which is explained by its weaker influence on the observed displacement field.

A comparison of the reconstruction error of the same functions using the collocation method and the projection method was performed. For smooth functions, the projection

Table 4. Comparison of reconstruction error for $\bar{\rho} = 1.3 + 2.6\eta - 2.2\eta^2$ using the collocation method and the projection method with 0.5% noise in the input information

Coordinate η	Exact value $\bar{\rho}$	Reconstructed value $\bar{\rho}$		Relative reconstruction error, %	
		Collocation method	Projection method	Collocation method	Projection method
0.6	2.07	2.24	2.15	8.2	3.9
0.64	2.06	2.21	2.13	7.3	3.4
0.68	2.05	2.18	2.11	6.3	2.9
0.72	2.03	2.08	2.07	2.5	2
0.76	2.0	2.04	2.03	2	1.5
0.8	1.97	2.0	1.98	1.5	1
0.84	1.93	1.96	1.92	1.6	0.5
0.88	1.88	1.75	1.86	6.9	1.1
0.92	1.83	1.72	1.78	6	2.7
0.96	1.77	1.65	1.7	6.8	4
1.0	1.7	1.54	1.61	9.4	5.3

method provides a reconstruction error 2–5 % lower than the collocation method. The comparison results for the test function $\bar{\rho} = 1.3 + 2.6\eta - 2.2\eta^2$ with 0.5 % noise are presented in Table 4. The projection method demonstrated higher stability to noise due to the smoothing property of approximation in the class of polynomials.

Conclusion

An iterative method for solving the coefficient inverse problem for a functionally graded elastic pipe with voids within the framework of the Cowin-Nunziato model is presented. Based on the weak formulation, Fredholm operator equations of the 1st kind are obtained, relating variations of the sought characteristics to the residual of displacement fields on the boundary. Two methods for discretizing the operator equations are proposed: (a) the collocation method (reconstruction at grid nodes); (b) the projection method (reconstruction in the class of polynomial functions) with a multi-stage refinement strategy. It has been established that the moduli $\bar{\mu}$ and $\bar{\rho}$ have the strongest influence, moduli $\bar{\lambda}$ and $\bar{\beta}$ have a moderate influence, and modulus $\bar{\xi}$ has a weak influence. This explains the different accuracy of their reconstruction. A detailed study of the method's stability to random errors in the input data was conducted. It is shown that for highly sensitive characteristics ($\bar{\mu}$, $\bar{\rho}$), the method is stable at a noise level of 1 %. For smooth functions, the projection method provides a reconstruction error 2–5 % lower than the collocation method with better noise stability.

A number of limitations of the proposed approach to solving inverse problems should be noted. First, the iterative process based on linearization requires a sufficiently close initial approximation to the exact (reconstructed) function. Second, the projection method is applicable only for reconstructing smooth functions, while for materials with discontinuous properties, the collocation method is preferable. Third, the reconstruction accuracy differs significantly for different moduli: the shear modulus and density are reconstructed with high accuracy, while the pore stiffness modulus is reconstructed with low accuracy due to its weak influence on boundary displacements. Fourth, at noise levels exceeding 1 %, the reconstruction accuracy of the moduli decreases significantly.

CRediT authorship contribution statement

Nesterov Sergey A. : writing – review & editing, writing – original draft; conceptualization.

Conflict of interest

The author declares no competing interests.

References

1. Chen D, Gao K, Yang J, Zhang L. Functionally graded porous structures: analyses, performances, and applications – A Review. *Thin-Walled Structures.* 2023;191: 111046.
2. Rudskoy AI, Popovich AA. *Functionally graded materials and additive technologies for their production.* St. Petersburg: Polytech press; 2022. (In Russian)
3. Hou C, Liu Y, Xu W, Lu X, Guo L, Liu Y, Tian S, Liu B, Zhang J, Wen C. Additive manufacturing of functionally graded porous titanium scaffolds for dental applications. *Biomater. Adv.* 2022;139: 213018.

4. Karimzadeh M, Basvoju D, Vakanski A, Charit I, Xu F, Zhang X. Machine Learning for Additive Manufacturing of Functionally Graded Materials. *Materials.* 2024;17(15): 3673.
5. Cowin SC, Nunziato JW. Linear elastic materials with voids. *Journal of Elasticity.* 1983;13: 125–147.
6. Cowin SC, Puri P. The classical pressure vessel problems for linear elastic materials with voids. *Journal of Elasticity.* 1983;13: 157–163.
7. Repka M, Sladek V, Sladek J. Numerical Analysis of Poro-elastic Materials Described by the Micro-dilatation Theory. *Procedia Engineering.* 2017;190: 248–254.
8. Li Y, Volkov VA, Rabinskiy NL, Shemiakov OA. Numerical modeling of scale effects for circular cylinder in the theory of thermoelastic materials with voids. *Journal of Applied Engineering Science.* 2020;18(4): 671–675.
9. Sha M, Volkov AV, Orekhov AA, Kuznetsova EL. Micro-dilatation effects in a two-layered porous structure under uniform heating. *Journal of the Balkan Tribological Association.* 2021;27(2): 280–294.
10. Nesterov SA. On the deformation of composite elastic bodies with empty pores. *Ecological Bulletin of Research Centers of the Black Sea Economic Cooperation.* 2025;22(1): 68–79. (In Russian)
11. Ieşan D, Scalia A. On the Deformation of Functionally Graded Porous Elastic Cylinders. *Journal of Elasticity.* 2007;87: 147–159.
12. Vatulyan AO, Shvedov DS. Oscillation of inhomogeneous poroelastic layer with voids. *Vestnik Don State Technical University.* 2013;13(1–2): 49–57. (In Russian)
13. Chiriţă S. Rayleigh Waves on an Exponentially Graded Poroelastic Half Space. *Journal of Elasticity.* 2013;110: 185–199.
14. Ramezani H, Steeb H, Jeong J. Analytical and numerical studies on penalized micro-dilatation (PMD) theory: macro-micro link concept. *European Journal of Mechanics, A/Solids.* 2012;34: 130–148.
15. Jeong J, Ram´ezani H, Sardini P, Kondo D, Ponson L, Siitari-Kauppi M. Porous media modeling and micro-structurally motivated material moduli determination via the micro-dilatation theory. *Eur. Phys. J. Special Topics.* 2015;224: 1805–1816.
16. Bishay PL, Repka M, Sladek V, Sladek J. On the characterization of porosity-related parameters in micro-dilatation theory. *Acta Mech.* 2017;228: 1631–1644.
17. Chebakov MI, Kolosova EM. Methodology of Determination of Porosity Parameters in the Theory of Microdilation. In: Parinov IA, Chang SH, Putri EP. (Eds.) *Physics and Mechanics of New Materials and Their Applications. PHENMA 2023. Springer Proceedings in Materials, vol 41.* Cham; Springer: 2024. p.335–344.
18. Vatul'yan AO, Lyapin AA. On inverse coefficient problems of poroelasticity. *Mechanics of Solids.* 2013; 48(2): 210–215.
19. Dudarev VV, Mnukhin RM, Vatulyan AO, Nedin RD, Gusakov DV. On the Determination of the Biot Modulus of Poroelastic Cylinder. *ZAMM - Journal of Applied Mathematics and Mechanics.* 2019;99(3): e201800137.
20. Vatulyan AO, Nesterov SA. On some features of identification of inhomogeneous prestressed state of thermoelastic hollow cylinder with coating. *Materials Physics and Mechanics.* 2019;42(1): 54–64.
21. Vatulyan AO, Nesterov SA. On Determination of the Thermomechanical Characteristics of a Functionally Graded Finite Cylinder. *Mechanics of Solids.* 2021;56(7): 1429–1438.
22. Vatul'yan AO, Nesterov SA. Study of the Inverse Problems of Thermoelasticity for Inhomogeneous Materials. *Siberian Mathematical Journal.* 2023;64(3): 699–706.
23. Vatulyan A, Nesterov S, Nedin R. Variable properties reconstruction for functionally graded thermoelectroelastic cylinder. *Continuum Mechanics and Thermodynamics.* 2024;36: 745–762.
24. Lyapin AA, Rudenko OV, Svyatko YuA. On the application of genetic algorithms and gradient methods for problem of initial stress field reconstruction in poroelastic inhomogeneous column. *Vestnik of Saint Petersburg University. Series 1. Mathematics. Mechanics. Astronomy.* 2016;3(3): 481–488. (In Russian)
25. Lecampion B, Constantinescu A. Sensitivity analysis for parameter identification in quasi-static poroelasticity. *Int. J. Numer. Anal. Meth. Geomech.* 2005;29: 163–185.
26. Dehghani H, ZilianA. Poroelastic model parameter identification using artificial neural networks: on the effects of heterogeneous porosity and solid matrix Poisson ratio. *Computational Mechanics.* 2020;66: 625–649.
27. Korobov P, Alekseev V. Numerical solution of a one-dimensional inverse retrospective problem for a system of poroelasticity equations. *Bulletin of the Novosibirsk Computing Center. Series: Mathemaical Modeling in Geophysics.* 2021;23: 19–24.
28. Imomnazarov KhKh, Khujaev LKh, Yangiboev ZSh. On inverse dynamic poroelasticity problem for layered medium. *Mat. Zamet. SVFU.* 2022;29(2):19–30. (In Russian)
29. Liu T. Porosity reconstruction based on Biot elastic model of porous media by homotopy perturbation method. *Chaos Solitons & Fractals.* 2022;158: 112007.
30. Krylov VI, Skoblya NS. *Approximate Fourier Transform and Laplace Transform Inversion Methods.* Moscow: Nauka; 1974. (In Russian).
31. Tikhonov AN, Arsenin VYa. Methods for the Solutioin of Ill-Posed Problems. Moscow: Nauka; 1986. (In Russian).